NIH Public Access
Author Manuscript
Neuron. Author manuscript; available in PMC 2015 May 07.

Published in final edited form as:
Neuron. 2014 May 7; 82(3): 603–617. doi:10.1016/j.neuron.2014.03.003.

Stepwise Recruitment of Transcellular and Paracellular Pathways Underlies Blood-Brain Barrier Breakdown in Stroke

Daniel Knowland[1,8], **Ahmet Arac**[2,3,8], **Kohei Sekiguchi**[4,5], **Martin Hsu**[1], **Sarah E. Lutz**[1], **John Perrino**[6], **Gary K. Steinberg**[2], **Ben A. Barres**[7], **Axel Nimmerjahn**[4,9,10], and **Dritan Agalliu**[1,9,10]

[1]Department of Developmental and Cell Biology, University of California, Irvine, CA 92697

[2]Department of Neurosurgery, Stanford University School of Medicine, Stanford, CA 94305

[3]Department of Medicine, University of California at Irvine, Orange, CA 92868

[4]Waitt Advanced Biophotonics Center, The Salk Institute for Biological Sciences, La Jolla, CA 92037

[5]Biological Sciences Graduate Program, University of California, San Diego, La Jolla, CA 92037

[6]Electron Microscopy Facility, Stanford University School of Medicine, Stanford, CA 94305

[7]Department of Neurobiology, Stanford University School of Medicine, Stanford, CA 94305

SUMMARY

Brain endothelial cells form a paracellular and transcellular barrier to many blood-borne solutes via tight junctions (TJs) and scarce endocytotic vesicles. The blood-brain barrier (BBB) plays a pivotal role in the healthy and diseased CNS. BBB damage after ischemic stroke contributes to increased mortality, yet the contributions of paracellular and transcellular mechanisms to this process *in vivo* are unknown. We have created a novel transgenic mouse strain whose endothelial TJs are labeled with eGFP and have imaged dynamic TJ changes and fluorescent tracer leakage across the BBB *in vivo*, using two-photon microscopy in the t-MCAO stroke model. Although barrier function is impaired as early as 6 h post-stroke, TJs display profound structural defects only after two days. Conversely, the number of endothelial caveolae and transcytosis rate increase as early as 6 h post-stroke. Therefore, stepwise impairment of transcellular followed by paracellular barrier mechanisms accounts for the BBB deficits in stroke.

© 2014 Elsevier Inc. All rights reserved.

[10]Correspondence: dagalliu@uci.edu and animmerj@salk.edu.
[8]These first authors contributed equally to this work
[9]These senior authors contributed equally to this work

SUPPLEMENTAL DATA
The supplemental data comprise seven supplemental figures (Figures S1–S7) linked to Figures 1–4, 6–8, one supplemental table (Table S1) and eight movies (Movie S1–S8), and can be found with this article online.

Publisher's Disclaimer: This is a PDF file of an unedited manuscript that has been accepted for publication. As a service to our customers we are providing this early version of the manuscript. The manuscript will undergo copyediting, typesetting, and review of the resulting proof before it is published in its final citable form. Please note that during the production process errors may be discovered which could affect the content, and all legal disclaimers that apply to the journal pertain.

NIH-PA Author Manuscript
NIH-PA Author Manuscript
NIH-PA Author Manuscript

NIH-PA Author Manuscript

NIH-PA Author Manuscript

NIH-PA Author Manuscript

INTRODUCTION

Stroke is a complex and devastating neurological condition that is the fourth-leading cause of death and primary reason for disability in the U.S. (Go et al., 2013). Although several processes that cause ischemic damage to neurons, glia and brain microvessels during ischemic stroke have been described, the response of the neurovascular unit (NVU) to this disease is poorly understood (del Zoppo, 2010; Arai et al., 2011). In particular, the precise cell biological mechanisms that impair blood-brain barrier (BBB) integrity *in vivo* following stroke are unknown. Endothelial cells (ECs) that survive in the perinfarct region, but do not maintain BBB properties, facilitate damage to the adjacent parenchyma and exacerbate the clinical prognosis. Thus it is crucial to understand how ECs respond *in vivo* to ischemic injury in order to develop therapies that may halt disease progression (Gursoy-Ozdemir et al., 2012).

ECs are crucial components of the ischemic response, because they normally create a barrier that limits diffusion of blood-borne solutes. There are three critical characteristics of brain endothelium that establish this barrier: 1) tight junctions (TJs) that restrict diffusion of molecules; 2) a small number of endocytotic vesicles and lowered rates of transcytosis relative to peripheral vasculature; and 3) active transport of molecules between blood and brain (Abbott et al., 2010). TJs restrict paracellular diffusion of ions between ECs, leading to the high transendothelial electrical resistance (TEER) of the BBB (Brightman and Reese, 1969; Butt et al., 1990). Claudin5 and -12, the major functional constituents of endothelial TJs, create size- and charge-selective hydrophilic paracellular pores (Morita et al., 1999; Anderson and Van Itallie, 2009), and Claudin5 plays an essential role in paracellular permeability to small molecules (<800 Da) at the BBB (Nitta et al., 2003). During the reperfusion following ischemic stroke, there is a biphasic increase in BBB permeability that contributes directly to cerebral vasogenic edema, hemorrhage and increased mortality.

The prevailing model suggests that active disassembly and reassembly of TJ protein complexes in CNS ECs accounts for both phases of BBB breakdown during reperfusion (Sandoval and Witt, 2008; Luissint et al., 2012). Hypoxic conditions alter both expression levels and localization of Claudin5, and reduce TEER in brain EC lines or isolated microvessels *in vitro*. Enzymatic degradation of the extracellular matrix by leukocyte-derived matrix metalloproteinases (MMPs), release of inflammatory cytokines within the ischemic core or peri-infarct area and secretion of vascular endothelial growth factor (VEGF) have all been postulated to trigger TJ disassembly during reperfusion (Rosenberg and Yang, 2007; Arai et al., 2011; Lakhan et al., 2013). Although defective TJ morphology has been reported as early as 3 h post-ischemia in rodents in conjunction with reduced levels of Claudin5, Occludin and Zona Occludens-1 (ZO-1), ultrastructural analysis of TJs during disease progression has produced no convincing evidence that TJ disruption is responsible for the early phase of BBB breakdown (Lossinsky and Shivers, 2004; Jiao et al., 2011; Krueger et al., 2013). On the contrary, TJ morphology remains normal even after 25 h of cerebral ischemia following embolic Middle Cerebral Artery Occlusion (MCAO), despite profuse extravasation of tracers from blood vessels (Krueger et al., 2013). These findings suggest that active remodeling of TJ complexes may occur in the late phase of reperfusion, when angiogenesis of CNS vessels begins (Arai et al., 2009).

NIH-PA Author Manuscript

NIH-PA Author Manuscript

NIH-PA Author Manuscript

In addition to the paracellular barrier, CNS blood vessels also provide a transcellular barrier by virtue of their small number of endocytotic caveolae having a low rate of transcytosis (Nag, 2003). Ultrastructural analysis suggests that enhanced transcellular transport may be the initial response of the CNS endothelium in stroke. This alternative mechanism for BBB opening involves upregulation in the number of endocytotic vesicles, which have been visualized by transmission electron microscopy (TEM) in conjunction with increased uptake of tracers by ECs in several stroke models (Ito et al., 1980; Dietrich et al., 1987; Cipolla et al., 2004; Lossinsky and Shivers, 2004). This mechanism of barrier disruption has to date been largely overlooked. Caveolae are intermediaries in the endocytotic pathway and contain receptors for proteins that must cross the BBB (Simionescu et al., 2009). Both expression of Caveolin1 (Cav1) and its phosphorylation state are increased as early as 2 h after CNS injury, prior to disassembly of TJ complexes and BBB breakdown (Nag et al., 2007). Cav1 interacts with Claudins and Occludin (Itallie and Anderson, 2012), and can influence their intracellular trafficking in response to inflammation (Stamatovic et al., 2009; Marchiando et al., 2010; Liu et al., 2012a). Despite the paramount role that BBB impairment plays in stroke, it is unclear whether increased endothelial caveolae at early phases of reperfusion precedes TJ remodeling *in vivo*, and whether these two cell biological mechanisms regulating transcellular and paracellular barrier properties are connected.

To address these issues, we have created a novel transgenic mouse strain, *Tg eGFP-Claudin5*, expressing a fusion of eGFP with Claudin5 in all CNS ECs. We have measured changes in structural TJ protein localization and BBB permeability in the transient MCAO (t-MCAO) model for stroke by performing two-photon, time-lapse microscopy (Nimmerjahn et al., 2009; Nimmerjahn, 2012c) in the cortex of anesthetized *Tg eGFP-Claudin5* mice, together with intravenous injection of fluorescent tracers. We find that TJs are stable during early phases of reperfusion, up to 24 h post-t-MCAO, but undergo significant remodeling and localization changes starting at 48–58 h post-t-MCAO, a relatively late time point *after* BBB breakdown. We corroborate these findings by immunofluorescence and TEM, which reveal decreased expression levels of Occludin and ZO-1 as well as ultrastructural changes in endothelial TJs at late stages of reperfusion. In contrast, the number of endothelial caveolae and rates of endocytosis and transcytosis are found to increase as early as 6 h post-t-MCAO, and to *precede* both disruption of TJ morphology and enhanced paracellular BBB permeability. Moreover, in *Cav1*-deficient mice, we find that transcellular but not paracellular permeability of cortical blood vessels is reduced following t-MCAO, suggesting that Cav1 regulates changes in transcellular but not paracellular endothelial barrier properties in response to stroke.

RESULTS

Transgenic BBB reporter mice and live imaging of normal barrier

To correlate structural alterations in TJs at the barrier with functional changes in vessel permeability, we created a novel transgenic mouse strain expressing a fusion of eGFP with Claudin5 protein in all ECs, under control of the endothelial *Tie-2/Tek-1* promoter/enhancer (Evans et al., 2000) (Figure 1A). We examined the expression and distribution of eGFP-Claudin5 protein in brain, retina, liver and muscle of this strain. The fusion protein localizes

NIH-PA Author Manuscript

NIH-PA Author Manuscript

NIH-PA Author Manuscript

to cell junctions of brain and retinal blood vessels by confocal and *in vivo* two-photon microscopy (Figure 1B–F), and colocalizes with the barrier-specific, TJ-associated proteins Occludin and ZO-1 (Figure 1J–M). However, eGFP-Claudin5 is retained predominantly in the secretory pathway of liver and muscle endothelial capillaries, but not larger caliber vessels (Figures S1A–B′), suggesting that CNS ECs regulate proper localization of the fusion protein to cell junctions.

We compared eGFP-Claudin5 protein levels to endogenous Claudin5 in brain and liver blood vessels, using quantitative infrared Western blotting. The *Tg eGFP-Claudin5* mice have a two-fold increase in total Claudin5 levels as compared to wild-type mice, with equal amounts of the endogenous and fusion proteins (Figure 1G–I); yet have similar levels of Occludin, Cav1 and the BBB transporter Slc2a1 (Glut-1) proteins with wild-type littermates (Figure S1D–F; data not shown). A small fraction (~4.7%) of myeloid and lymphoid lineage cells in *Tg eGFP-Claudin5* mice are also eGFP-positive (Figure S1C, Table S1). Since Claudin5 regulates BBB paracellular permeability (Nitta et al., 2003), we determined whether expression of the fusion protein in ECs impairs vascular permeability to small molecules in the CNS or other organs. We examined the biodistribution of a small molecular weight (MW) fluorescent tracer, 5-(and-6-) tetramethylrhodamine biocytin (biocytin-TMR, MW = 869 Da) following tail vein injection into healthy *Tg eGFP-Claudin5* or wild-type animals. Biocytin-TMR ordinarily crosses the BBB only when paracellular permeability is enhanced (Baur and Baumgartner, 2000) since the Na^+-dependent multivitamin transporter *Slc5a6*, responsible for biotin transport, is not expressed by CNS ECs (Daneman et al., 2010a; Ohkura et al., 2010). We found that biocytin-TMR is absent from brains of transgenic mice but distributed at levels similar to those of wild-type littermates in liver, muscle and other organs (Figure S1G–I; data not shown). Therefore, overexpression of eGFP-Claudin5 protein in blood vessels does not decrease the paracellular permeability of non-CNS vasculature.

Delayed appearance of TJ structural abnormalities in *Tg eGFP-Claudin5* cortical endothelium after stroke

Using *in vivo* two-photon microscopy we imaged TJs in parietal cortex blood vessels from anesthetized *Tg eGFP-Claudin5* transgenic mice prepared with either a cranial window and intact *dura mater* or a polished and reinforced thinned skull window (diameter 1.5–2.0 mm) (Nimmerjahn, 2012c). We combined TJ imaging in CNS capillaries with injection of two tracers biocytin-TMR (~870 Da) or dextran-TMR (3 kDa), to correlate structural changes in TJ protein localization with functional integrity of the BBB as measured by tracer diffusion into the CNS parenchyma. In healthy animals with a cranial window we found that TJs are stable, and both tracers remained confined within the vessel lumen (Figure 2C; Movie S1; data not shown). However, a small fraction (~4.5%) of $eGFP^+$ TJ strands (see definition in Methods section) contained small gaps (TJ strand discontinuities of at least ~0.4 μm in length) or protrusions (bulbous extensions from an otherwise linear TJ strand within the endothelial cell; Figure 2K–O), two structural features that are found during TJ remodeling (Shen et al., 2008).

NIH-PA Author Manuscript

NIH-PA Author Manuscript

NIH-PA Author Manuscript

We next examined changes in TJ localization and BBB functional impairment during stroke progression *in vivo* with two-photon microscopy, using the t-MCAO model. Previous studies had suggested that dynamic disassembly and reassembly of endothelial TJs accounts for the biphasic opening of the BBB in stroke (Sandoval and Witt, 2008); however an *in vivo* dynamic analysis of this process is lacking. We subjected 8–20 week-old transgenic mice to t-MCAO for 45 min (Arac et al., 2011), then imaged changes in endothelial TJ strands and leakage of tracers across the damaged barrier, in 120–240 μm thick cortical volumes within the stroke core area during a 6–58 h time period post-t-MCAO (Figure 2A–B, D–F; Movie S2; data not shown). We quantified the percentage of $eGFP^+$ TJ strands that contain gaps or protrusions as a measure of TJ disassembly and remodeling. We found that a significant fraction (34.3%) of $eGFP^+$ TJ strands had large gaps, ranging from 0.5–4.0 μm, by 48–58 h post-t-MCAO, compared to 7.5% and 9% at 12–14 h and 24–30 h post-t-MCAO, respectively, or healthy controls (4.5%) (Figure 2G–J, M; $p < 0.0001$). In addition, many $eGFP^+$ TJs strands in venules (22%), but not capillaries, had multiple protrusions at 48–58 h post-t-MCAO (Figure 2J, K, N, O) and an aberrant zigzag appearance (Figure 2L) reminiscent of ZO-1/2-deficient epithelial cells (Umeda et al., 2006). These data suggest that TJs undergo remodeling and structural changes predominantly between 48–58 h post-t-MCAO.

To examine whether structural abnormalities between endothelial TJs are dynamic in healthy cortex or within the core and penumbra regions during stroke progression, we subjected 8–20 week-old mice to continual two-photon time-lapse imaging over many days. These mice had a polished, reinforced thinned-skull window (Drew et al., 2010) and were imaged before and at three time points after a 45 min t-MCAO. Each recording session lasted ~2 h with repeated optical recordings (every 15–25 min) from distinct cortical volumes (Figure 3A). This allowed us to follow the same cortical blood vessels in healthy or stroke animals over multiple days, and to quantify changes in endothelial TJ strands and leakage of biocytin-TMR (Figure S3A–E). While the relationship between large and small vessels did not change in controls, stroke animals showed major vessel rearrangements during stroke progression, likely due to tissue edema (Figure S3B–E). Vessel rearrangements included shifts of the cortical with respect to dura vessels, which sometimes impaired recordings from previously imaged structures, and changes in intracortical vessel orientation that altered the angle at which these vessels were viewed across imaging sessions. Such vessels were excluded from our analysis. We analyzed dynamic changes in protrusions and gaps in endothelial TJs for both capillaries and venules. Consistent with our cranial window observations, we found fewer TJ protrusions in capillaries compared to venules in both healthy and stroke animals (Figure 2N, O). Over shorter time periods (2 h), the majority of protrusions were very stable in healthy capillaries and venules (the fraction of dynamic protrusion in TJ venules was 5–13%, n = 4 animals and 3 time-lapse series/animal). However, these protrusions moved at a longer time scale (Figures 3B–C and F–G, yellow and red arrows; Movies S3–4). In contrast, TJ protrusions in venules from stroke core and penumbra cortical regions were highly dynamic during both short and prolonged time periods, in particular at 48–58 h post-t-MCAO (the fraction of dynamic protrusion in TJ venules within the stroke core was 50–100%, n = 5 animals, and 25–54% within the penumbra region at both time points, n = 4 animals, 3 time-lapse series/animal; Figures 3D–

NIH-PA Author Manuscript

NIH-PA Author Manuscript

NIH-PA Author Manuscript

E and H–I; Figure S3F–I; Movies S5–S8). In contrast, gaps appeared abruptly within endothelial TJ strands at later stages of t-MCAO, and they were present throughout the duration of individual two-hour imaging sessions even at 48–58 h post-t-MCAO (Figure 3J, K, green arrows). These findings suggest that protrusions, but not gaps, are highly dynamic structures that likely reflect active TJ remodeling processes.

We determined the fractional biocytin-TMR and vascular IgG leakage area (i.e. stroke-affected area) in sections along the rostrocaudal axis following t-MCAO, and assessed the ratio of the average biocytin-TMR or IgG pixel intensity for ipsilateral (iCtx) or contralateral (cCtx) parietal cortex using wild-type and *Tg eGFP-Claudin5* animals, from 6–58 h post-t-MCAO. There was a gradual, significant increase in the biocytin-TMR and IgG leakage areas from 6–58 h post-t-MCAO for all rostrocaudal regions of the brain (Figure S2A–H, I, K; $p<0.0001$). However, biocytin-TMR and IgG average pixel intensities in the ipsilateral parietal cortex were significantly increased only 24–30 h and 48–58 h post-t-MCAO when compared to healthy mice (Figure 2E, F; S2J, L; $p<0.0001$). The progressive increase in the biocytin-TMR or IgG leakage areas, as well as their average pixel intensity within the ipsilateral cortex over time, was comparable between wild-type and *Tg eGFP-Claudin5* mice from 6–58 h post-t-MCAO (Figure S2I–L). Similar results were obtained using dextran 3kDa-TMR (data not shown). Therefore, the fusion protein does not modify the pathological progressive increase in endothelial paracellular permeability in response to stroke. We next examined eGFP-Claudin5, Occludin and ZO-1 expression at several time points post-t-MCAO, in either healthy or ipsilateral cortex. Occludin and ZO-1 colocalize with eGFP at endothelial TJs up to 24–30 h post-t-MCAO, similar to the healthy animals (Figure S4A–C″, E–G″). However, eGFP had a predominantly intracellular, rather than junctional, localization in ECs labeled with BSL-rhodamine by 48–58 h post-stroke, which is consistent with reduced Occludin and ZO-1 expression in blood vessels (Figure S4D–D″, H–H″). In addition, the endothelial basement membrane proteins Collagen IV, Laminin-α2 and Nidogen were also reduced at 48 h post-t-MCAO (Figure S4I–L; data not shown). Therefore, the abundant eGFP-positive TJ strands having structural abnormalities *in vivo* between 48–58 h post-t-MCAO mirror the loss of TJ protein expression in the ipsilateral cortex, as well as the abundant tracer and endogenous IgG leakage into the parenchyma.

We also examined ultrastructural changes in TJ morphology by TEM in *Tg eGFP-Claudin5* mice during stroke progression. Some TJs in ipsilateral cortical blood vessels (venules and capillaries) within the stroke core region had an abnormal appearance; TJs exhibited gaps where adjacent EC membranes had lost contact with each other (Figure 4C–F). The membrane around the gaps lacked electron dense material, suggesting absence of TJ proteins. These structural aberrations were rarely found in healthy or contralateral cortex (Figure 4A, B). The fraction of abnormal TJs with gaps was highly significant only at 48–58 h post-stroke but not earlier (Figure 4G; 46.1%; $p<0.0001$). In addition, TJ gaps became progressively larger between 24–58 h post-t-MCAO, ranging in diameter from 0.2 to 1.2 μm (Figure 4E, F). Therefore, severe ultrastructural TJ abnormalities in the late phase (48–58 h) closely correlate with the structural defects found by *in vivo* two-photon imaging.

NIH-PA Author Manuscript

NIH-PA Author Manuscript

NIH-PA Author Manuscript

Endothelial caveolae numbers and transcytosis rates increase at early phases of t-MCAO

Because structural abnormalities in endothelial TJs appear at a delayed phase of BBB impairment (48–58 h; Figure 2M, N) and correlate with a delay in tracer leakage (Figure S2J, L), we examined whether changes in endocytosis and transcytosis rates might account for the early rise in BBB permeability during reperfusion. Using both TEM and immune-electron microscopy for Cav1, we determined the number of caveolae in healthy or diseased ECs at various stages post-t-MCAO. The average number of caveolae in each immuno-EM image was significantly increased in the ipsilateral cortex as early as 6 h post-t-MCAO, compared to contralateral stroke cortex (Figure 5A–C, G–I, M; $p<0.0001$). In addition, the size of Cav1-positive vesicles was increased up to 200 nm (from 50–70 nm in healthy tissue) as early as 6 h post-t-MCAO in the ipsilateral cortex. The number and size of caveolae per EC in sections remained significantly higher than controls at 12–58 h post-stroke (Figure 5D–F, J–M). Moreover, a larger fraction of $Cav1^+$ vesicles were found in the basal side of the endothelial cells in the ipsilateral cortex 6 h post-t-MCAO, suggesting that trafficking of these vesicles inside the cell had changed (Figure 5N). Therefore, ECs respond to ischemic insult by increasing the number of their caveolae as early as 6 h post-t-MCAO, consistent with previous findings (Cipolla et al., 2004; Lossinsky and Shivers, 2004).

We next examined whether the increased endothelial caveolae in early phases of reperfusion reflects an increase in the rates of endocytosis and transcytosis. We analyzed uptake and transport of fluorescently labeled albumin (alb-Alexa594) across ECs in either healthy or stroke cortex, since it crosses the BBB by receptor-mediated transcytosis/endocytosis or fluid phase absorption (Schubert et al., 2001; Tiruppathi et al., 2004). We injected *Tg eGFP-Claudin5* or wild-type mice with 1% alb-Alexa594, and 30 min after injection measured the amount present in either brain ECs and parenchyma at various time points (Figure 6A, B). The fraction of either the $Glut1^+$ or BSL^+ EC area that was filled with tracer-positive vesicles was significantly higher in ipsilateral stroke cortical vessels as early as 6 h post-t-MCAO (37.8%) compared to healthy vessels (4.7%) (Figure 6E–H, O; S5A–I). The fraction of tracer uptake in ipsilateral stroke endothelium was reduced to 24% by 12–30 h post-t-MCAO, but returned to 37% by 48–58 h; this is likely due to upregulation in endothelial endocytosis in the second phase of enhanced BBB permeability (Figure 6I–O, S5I). In addition, the number of alb-Alexa594-positive vesicles within the brain parenchyma area was significantly higher in ipsilateral stroke cortical vessels at both 6 h and 48 h post-t-MCAO, compared to healthy vessels (Figure 6P; S5J). Taken together, the increased caveolae numbers and alb-Alexa594 uptake in cortical endothelium and transport within the brain parenchyma, as early as 6 h post-t-MCAO, suggest that upregulation of both endothelial endocytosis and transcytosis accounts for the initial impaired barrier function during reperfusion.

Mice lacking Caveolin1 have reduced transcellular but not paracellular permeability in cortical vessels after t-MCAO

To assess whether disruption of TJ structural integrity and the increase in paracellular permeability at later phases depends on upregulation of transcytosis at early stages, we analyzed both endothelial uptake and transport into brain parenchyma of alb-Alexa594 6 h and 27 h following t-MCAO, as well as diffusion of biocytin-TMR across cortical blood

NIH-PA Author Manuscript

NIH-PA Author Manuscript

NIH-PA Author Manuscript

vessels at 27 h, in either wild-type or *Cav1*-deficient mice that lack EC caveolae (Drab et al., 2001; Razani et al., 2001). The mean percentage of Glut1^{+} or BSL^{+} blood vessel surface area filled with alb-Alexa594 and the amount of tracer transported into the brain parenchyma was significantly reduced within the ipsilateral cortex of *Cav1*$^{-/-}$ mice compared to wild-type controls, at both 6 h and 27 h post-t-MCAO (Figure 7A–H; S6A, B; data not shown). Some (22–25%) alb-Alexa594 was endocytosed in liver or stroke ECs in *Cav1*-deficient mice; these data conflict with previous studies suggesting that Cav1 is required for albumin transport across lung ECs (Schubert et al., 2001), but may be explained by Cav1-independent endocytosis. We find that a large fraction of alb-Alexa594 vesicles colocalize with EEA1^{+} early endosomes but not LAMP1^{+} lysosomes or Rab7^{+} late endosome markers in primary brain ECs (Figure S6C–G). Furthermore, more tracer-positive vesicles are present in the early endosome when primary brain ECs are cultured for 3 d under hypoxic conditions (Figure S6C′–G′), suggesting that alb-Alexa594-positive vesicles are routed toward the endosome during hypoxic stroke.

We then quantified the biocytin-TMR or IgG leakage area in tissue sections from wild-type and *Cav1*-deficient mice 27 h after t-MCAO. We found that the percentage of the tracer leakage area was significantly increased in *Cav-1*$^{-/-}$ (45.8%) compared to wild-type (37%) mice (Figure 8A–C; S7A–C; $p<0.0001$; Standard t-Test), as previously reported (Jasmin et al., 2007). This difference was largely due to selective biocytin-TMR or IgG extravasation within the ipsilateral thalamus (data not shown). Although the stroke area was increased in *Cav1*$^{-/-}$ compared to wild-type mice, the ratio of average biocytin-TMR or IgG pixel intensity between the ipsilateral and contralateral area was unchanged within anatomically matched CNS regions between the two strains (Figure 8D, S7D). Moreover, expression levels, subcellular localization of several TJ proteins (Claudin5, Occludin and ZO-1) and TJ ultrastructural morphology by TEM in healthy brain ECs are undistinguishable between *Tg eGFP-Claudin5 Cav-1*$^{-/-}$ mice and *Tg eGFP-Claudin5* littermates (Figure 8E–H, S7E–J), suggesting that Cav1 is not required for proper formation of CNS endothelial TJs as had been suggested (Schubert et al., 2002). Therefore, the increase in paracellular permeability observed in *Cav1*$^{-/-}$ CNS endothelium in stroke is not due to aberrant formation of TJs in the healthy brain, but is rather a normal physiological response of mutant endothelial cells to pathological stimuli. These findings suggest that Cav1 controls the transcellular but not paracellular mechanisms responsible for increased cortical blood vessel permeability in response to ischemic stroke.

DISCUSSION

Multiple components of the NVU respond rapidly and simultaneously to ischemic injury in a coordinated manner (del Zoppo, 2010). The sequence of endothelial cell biological mechanisms that impair BBB function during stroke *in vivo*, however, remains controversial (Lossinsky and Shivers, 2004; Sandoval and Witt, 2008). We have addressed this controversy with the generation of novel *Tg eGFP-Claudin5* transgenic mice and two-photon imaging in live animals, to examine structural changes in CNS endothelial TJs within the cortical core and peri-infarct areas in the t-MCAO model for stroke. We find that major TJ structural abnormalities occur at 48–58 h post-t-MCAO, a late phase of stroke progression. In addition, our study reveals that BBB disruption in response to ischemia

NIH-PA Author Manuscript

NIH-PA Author Manuscript

NIH-PA Author Manuscript

involves sequential activation of two distinct mechanisms, beginning with upregulation of endothelial transcytosis in the early phase of reperfusion (6 h) followed by major remodeling of TJ complexes in the late phase (24–48 h). The time scale for increased BBB permeability to tracers that primarily cross the barrier via transcellular rather than paracellular pathways matches the sequence of structural changes in ECs during reperfusion, suggesting that current models of how BBB disruption occurs in stroke must be reconsidered (Sandoval and Witt, 2008). Disruption of the paracellular barrier in gut epithelial cells in response to inflammation is also achieved by sequential activation of Cav1-mediated endocytosis followed by TJ remodeling (Marchiando et al., 2010). These cellular events may therefore represent a general principle for how tissues possessing barrier properties respond to injury.

Tg eGFP-Claudin5 transgenic mice as a genetic tool to study endothelial TJ dynamics and immune cell interactions in CNS disease

TJs have traditionally been viewed as stable structures (Brightman and Reese, 1969). However, imaging of eGFP-tagged TJ proteins, either in cultured cells or whole animals, has revealed a dynamic remodeling in both healthy and disease states (Shen et al., 2008; Marchiando et al., 2010). The BBB undergoes rapid changes in permeability in response to CNS insults, yet traditional approaches for studying barrier permeability do not provide either dynamic measurement of BBB breakdown during disease or correlation with structural endothelial abnormalities. To overcome this obstacle, we developed a transgenic mouse strain that expresses eGFP fused to the N-terminus of Claudin5 in ECs to maintain its interactions with ZO-1 (Piontek et al., 2008), and two-photon imaging assays for combined measurement of TJ dynamics and tracer leakage in cortical vessels *in vivo*. These *Tg eGFP-Claudin5* mice are a novel genetic tool to enable dynamic analysis of TJ formation in blood vessels during development, TJ junction breakdown associated with increased vascular permeability as well as dynamic interactions of the endothelium with either immune cells or parasites during CNS disease (Zlokovic, 2008).

Overexpressing eGFP-Claudin5 has the potential to affect endothelial barrier function, since Claudin5 levels are essential for size selectivity of the paracellular barrier (Nitta et al., 2003). However, we find no evidence for reduced permeability of non-CNS endothelium in healthy *Tg eGFP-Claudin5* compared to wild-type mice (Figure S1). Moreover, the gradual increase in endothelial paracellular permeability to small tracers (e.g. biocytin-TMR) or IgG following ischemic stroke is identical between transgenic and wild-type littermates. Finally, our analysis of structural changes in cortical endothelial TJs during stroke by two-photon microscopy correlates well with TJ structural aberrations identified by TEM and immunofluorescence. Therefore, *Tg eGFP-Claudin5* transgenic mice can be used to detect dynamic changes in endothelial TJs during disease.

Stepwise recruitment of transcellular and paracellular pathways accounts for changes in endothelial barrier properties during stroke progression

Despite the obvious clinical and therapeutic relevance, satisfactory mechanisms for how the NVU *in toto* responds to stroke, and how BBB integrity is impaired at the cell biological level, are lacking. Active disassembly and reassembly of TJ protein complexes has been considered to play a major role in the biphasic opening of the BBB during reperfusion

NIH-PA Author Manuscript

NIH-PA Author Manuscript

NIH-PA Author Manuscript

(Sandoval and Witt, 2008); however our data do not support this model. We find that major abnormalities within TJ strands (e.g. gaps or protrusions) are mostly present 48–58 h post-t-MCAO, corresponding to the second peak of biphasic increase in BBB permeability, while during the early phase of enhanced permeability, TJ strands are relatively normal in the ipsilateral stroke cortex. Our repeated time-lapse recordings within the same vessels before and after t-MCAO, demonstrate that protrusions are particularly dynamic 48 h after t-MCAO. Therefore, active remodeling of TJ proteins appears not to play an important role in increased BBB permeability during the early phase of reperfusion. Several additional lines of evidence support our conclusion. First, TEM and immunofluorescence assays for TJ morphology changes agree with our two-photon imaging data, arguing against a limitation in detecting early TJ defects by two-photon imaging. Second, while t-MCAO typically results in infarction of the basal ganglia with less severe deficits in the cerebral cortex, due to a compensatory circulatory system from surface-communicating arterioles (Schaffer et al., 2006), the parietal cortex area imaged was located within the stroke or penumbra region based on three criteria: a) early changes in endothelial caveolae and the rates of transcytosis visualized by TEM and tracer uptake, respectively; b) motor deficits in animals after recovery from t-MCAO (data not shown); and c) anatomical distribution of biocytin-TMR 6–58 h post-t-MCAO after dynamic imaging. Finally, the kinetics of biocytin-TMR or IgG extravasation during stroke do not mimic the well-characterized biphasic increase in BBB permeability measured with Evans blue in various animal models (Sandoval and Witt, 2008) since their endothelial permeability increases gradually between 20–58 h following t-MCAO (Figure 8I; blue and green lines), consistent with the appearance of TJ structural abnormalities. Normal TJs have also been found 25 h after ischemia in an embolic MCAO rat model (Krueger et al., 2013) suggesting that delayed TJ remodeling is a common feature of the CNS endothelial response to various forms of stroke.

What accounts for early changes in BBB permeability following ischemic stroke? Our structural analysis clearly demonstrates that the number of endothelial caveolae is increased as early as 6 h post-t-MCAO in the parietal cortex. These findings are consistent with reports that CNS ECs upregulate transcellular vesicular transport in response to hypertension and cerebral ischemia/stroke (Ito et al., 1980; Dietrich et al., 1987; Cipolla et al., 2004; Lossinsky and Shivers, 2004). Consistent with increased caveolae numbers, endothelial uptake and transport of alb-Alexa594 into the brain parenchyma is enhanced as early as 6 h post t-MCAO. The kinetics of alb-Alexa594 uptake during reperfusion follows the canonical biphasic increase in BBB permeability, with higher rates at 6 and 48–58 h and lower rates 12–30 h post-stroke (Figure 8I). Although Cav1 levels increase within the stroke core region post-t-MCAO (Jasmin et al., 2007), endothelial uptake of alb-Alexa594 following ischemia seems to be mediated by both Cav1-dependent and -independent endocytosis, since uptake is reduced but not completely abolished in *Cav1*−/− mice (Figure 7, S6). We propose that barrier permeability during reperfusion has two steps: 1) initial upregulation of endothelial transcytosis that accounts for the early peak in enhanced BBB permeability; and 2) delayed remodeling and disassembly of TJ protein complexes in the second phase that exacerbates barrier dysfunction, leading to progressive demise of the perinfarct area (Figure 8I). The selective reduction in transcellular but not paracellular permeability in cortical blood vessels of *Cav-1* deficient mice after stroke suggests that these two processes are regulated

NIH-PA Author Manuscript

NIH-PA Author Manuscript

NIH-PA Author Manuscript

independently. Since both expression and localization of several BBB TJ proteins are normal in healthy *Cav1*$^{-/-}$ CNS ECs, their increase in paracellular permeability during t-MCAO is not due to inherently defective TJs in *Cav1*$^{-/-}$ endothelial cells, but rather is a standard physiological response of the mutant endothelium to ischemia. It is possible that dynamic properties of endothelial TJs may be different between wild-type and *Cav1*$^{-/-}$ mice; however, dynamic imaging of TJs with pharmacological inhibition of transcytosis *in vivo* would not allow us to parse out its role in endothelial cells versus other components of the NVU.

Disruption of the paracellular barrier in gut epithelial cells in response to TNFα–induced inflammation is also mediated by an increase in Cav1-dependent endocytosis, followed by Occludin internalization and disruption of TJ strands (Marchiando et al., 2010). Pharmacological or genetic inactivation of Cav1 prevents TNFα-induced enhancement in paracellular permeability and TJ remodeling in gut epithelial cells, suggesting that these two processes are tightly linked (Marchiando et al., 2010). These findings contrast with our observations that endothelial paracellular permeability does not depend on Cav1 function in ischemic stroke. Such differences between endothelial and epithelial responses may be due to the inherent dissimilarity between these barriers, or may reflect distinct types of pathological insult (inflammation versus hypoxia).

Why do ECs respond initially during ischemic stroke by changing their rate of transcytosis? One potential explanation relies on the early separation and migration of pericytes away from brain microvessels within 2 h after focal cerebral ischemia, due to dissolution of the basement membrane (Dore-Duffy et al., 2000; Liu et al., 2012b). Pericytes regulate BBB formation and maintenance by secreting inhibitory signals that reduce the number of caveolae and rate of endothelial transcytosis (Armulik et al., 2010; Daneman et al., 2010b). Pericyte detachment may relieve an important inhibitory mechanism that is required to maintain low transcytosis in CNS blood vessels. However, it is unclear if increased endothelial transcytosis provides a beneficial signal to the NVU during the initial phase of stroke progression. Later, disruption of basement membranes by leukocyte-derived MMPs, the presence of major inflammatory cytokines in the stroke region, upregulation of endothelial eNOS signaling and production of angiogenic growth factors such as VEGF and angiopoietins can all lead to secondary dissolution of TJ structure and function and enhanced TJ remodeling (Arai et al., 2011). This process may function in parallel with upregulation of endothelial transcytosis to impair BBB function in ischemic stroke.

EXPERIMENTAL PROCEDURES

Generation of *Tg eGFP-Claudin5* transgenic mice

An N-terminal fusion of eGFP with mouse Claudin5 was inserted downstream of the 2.5 kb murine *Tie2/Tek1* promoter and upstream of a 10 kb enhancer that includes exon 1 (Evans et al., 2000). We obtained 8 founder lines, of which 2 (lines 4 and 15) showed strong expression throughout the vasculature. Line 15 was used for most experiments described in this study.

NIH-PA Author Manuscript

NIH-PA Author Manuscript

NIH-PA Author Manuscript

Mouse ischemic stroke model and two-photon *in vivo* imaging

All experimental procedures were approved by the IACUC committees at the University of California at Irvine, Stanford University and the Salk Institute for Biological Studies. 8- to 20-week-old male mice weighing 25–30 g were subjected to t-MCAO as described (Arac et al., 2011). Head plate implantation surgery was performed as described (Nimmerjahn, 2012b). For one-time imaging, a craniotomy was performed (typically 1.3–2.0 mm in diameter at around −1.0 mm post-bregma and 3.5 mm lateral) leaving the *dura mater* intact (Nimmerjahn, 2012a). For repeated imaging, a thinned skull window was prepared ~24 h prior to imaging [typically 1.0–1.5 mm in diameter at around −1.0 mm post-bregma and 3.5 mm lateral, reinforced with a #0 cover slip (Thomas Scientific)] (Drew et al., 2010). Blood plasma was labeled by tail vein injection of biocytin-TMR or 3,000 MW Dextran-TMR (1% in PBS). Imaging was performed on an upright two-photon microscope equipped with a pulsed femtosecond Ti:Sapphire laser (Chameleon Ultra II, Coherent or Tsunami, Spectra-Physics), two fluorescence detection channels and water-immersion objectives. Further details are provided in Supplementary Experimental Procedures.

Immunofluorescence and tracer leakage quantitation

Brains, muscle, liver and kidneys from C57BL6/J, *Tg eGFP-Claudin5, Cav1*$^{-/-}$, or *Tg eGFP-Claudin5 Cav1*$^{-/-}$ mice were harvested 30–45 min after tail vein injection with 1% biocytin-TMR or alb-Alexa594 solution (Life Technologies, CA). Brain or liver blood vessels were labeled by immunofluorescence with antibodies for Glut-1, BSL-FITC or BSL-Rhodamine. Streptavidin-Alexa594 (Life Technologies, CA) was used to visualize biocytin-TMR distribution in tissues. Sections were imaged with an upright Zeiss Axioimager and biocytin-TMR or IgG leakage was quantified with Fiji software. See Supplementary Experimental Procedures for more details.

Transmission electron microscopy (TEM) and immunoelectron microscopy (IEM)

TEM samples from either healthy, ipsilateral or contralateral stroke cortex were fixed in Karnovsky's fixative for 1 h at room temperature followed by overnight fixation at 4°C. For IEM, brains were fixed in 4% warm PFA for 6 h, sectioned and stained for Cav1 (1:1000) followed by incubation with Nanogold anti-rabbit IgG (1:50; Nanoprobes, NY). Gold particles were enhanced with the HQ Silver™ Enhancement Kit (Nanoprobes, NY). Stained sections were processed for TEM and imaged with a JEOL 1230 TEM at 80 kV. Photos were taken with a Gatan Orius digital camera. We obtained approximately 70 images of caveolae per sample. The numbers of Cav1^{+} vesicles visualized by IEM were counted from each image and averaged for each sample.

TJ quantitation

Maximum intensity projections were created for each image stack/3D recording volume in order to quantify TJ abnormalities in two-photon time-lapse data for each time point. We then determined the number and percentage of TJ strands with protrusions or gaps and the fraction of dynamic protrusions and gaps. Blood vessel borders were defined by the presence of tracers. To quantify TJ strands with abnormal morphology in EM data, we obtained approximately 70 images of TJs for each EM sample, counted the number of TJ

NIH-PA Author Manuscript

NIH-PA Author Manuscript

NIH-PA Author Manuscript

strands with abnormalities (gaps) per image and calculated the percent of abnormal versus total TJs (further details are found in Supplemental Experimental Procedures).

Supplementary Material

Refer to Web version on PubMed Central for supplementary material.

Acknowledgments

We thank the transgenic mouse facilities at our respective institutions for generating and rederiving *Tg eGFP-Claudin5* mice, Ilir Agalliu at Albert Einstein College of Medicine for help with statistical analysis, Tyler Cutforth for critical comments on the manuscript and Mark J. Schnitzer at Stanford University for accommodating our initial imaging experiments in his laboratory. D.A. was supported by grants from the AHA (12BGIA11560014), NMSS (RG4673A1/1) and NIH (1R01 HL116995-01); A.N was supported by grants from the Rita Allen Foundation, Whitehall Foundation and NIH (New Innovator Award, 1DP2NS083038; Cancer Center Core Grant, P30 CA014195-40); K.J.S. was supported by funds from the Nakajima, Mary J. Chapman and Jesse and Caryl Philips Foundations; A.A. was supported by a Stanford University School of Medicine Dean's Fellowship; G.K.S. was supported by grants from the NIH (1P01NS37520-08) and the Russell and Elisabeth Siegelman, Bernard and Ronni Lacroute and William Randolph Hearst Foundations; B.A. was supported by grants from the NMSS (RG3936A7/1; RG3936BG/1) and the Myelin Repair Foundation.

References

Abbott N, Patabendige A, Dolman D, Yusof S, Begley D. Structure and function of the blood-brain barrier. Neurobiology of Disease. 2010; 37:13–25. [PubMed: 19664713]

Anderson JM, Van Itallie CM. Physiology and function of the tight junction. Cold Spring Harbor perspectives in biology. 2009; 1:a002584. [PubMed: 20066090]

Arac A, Brownell SE, Rothbard JB, Chen C, Ko RM, Pereira MP, Albers GW, Steinman L, Steinberg GK. Systemic augmentation of alphaB-crystallin provides therapeutic benefit twelve hours post-stroke onset via immune modulation. Proceedings of the National Academy of Sciences of the United States of America. 2011; 108:13287–13292. [PubMed: 21828004]

Arai K, Jin G, Navaratna D, Lo EH. Brain angiogenesis in developmental and pathological processes: neurovascular injury and angiogenic recovery after stroke. Febs J. 2009; 276:4644–4652. [PubMed: 19664070]

Arai K, Lok J, Guo S, Hayakawa K, Xing C, Lo EH. Cellular mechanisms of neurovascular damage and repair after stroke. J Child Neurol. 2011; 26:1193–1198. [PubMed: 21628695]

Armulik A, Genove G, Mae M, Nisancioglu MH, Wallgard E, Niaudet C, He L, Norlin J, Lindblom P, Strittmatter K, et al. Pericytes regulate the blood-brain barrier. Nature. 2010; 468:557–561. [PubMed: 20944627]

Baur B, Baumgartner ER. Biotin and biocytin uptake into cultured primary calf brain microvessel endothelial cells of the blood-brain barrier. Brain Res. 2000; 858:348–355. [PubMed: 10708686]

Brightman MW, Reese TS. Junctions between intimately apposed cell membranes in the vertebrate brain. J Cell Biol. 1969; 40:648–677. [PubMed: 5765759]

Butt AM, Jones HC, Abbott NJ. Electrical resistance across the blood-brain barrier in anaesthetized rats: a developmental study. The Journal of physiology. 1990; 429:47–62. [PubMed: 2277354]

Cipolla MJ, Crete R, Vitullo L, Rix RD. Transcellular transport as a mechanism of blood-brain barrier disruption during stroke. Front Biosci. 2004; 9:777–785. [PubMed: 14766407]

Daneman R, Zhou L, Agalliu D, Cahoy JD, Kaushal A, Barres BA. The mouse blood-brain barrier transcriptome: a new resource for understanding the development and function of brain endothelial cells. PLoS One. 2010a; 5:e13741. [PubMed: 21060791]

Daneman R, Zhou L, Kebede AA, Barres BA. Pericytes are required for blood-brain barrier integrity during embryogenesis. Nature. 2010b; 468:562–566. [PubMed: 20944625]

del Zoppo GJ. The neurovascular unit in the setting of stroke. J Intern Med. 2010; 267:156–171. [PubMed: 20175864]

NIH-PA Author Manuscript

NIH-PA Author Manuscript

NIH-PA Author Manuscript

Dietrich WD, Busto R, Watson BD, Scheinberg P, Ginsberg MD. Photochemically induced cerebral infarction. II. Edema and blood-brain barrier disruption. Acta Neuropathol. 1987; 72:326–334. [PubMed: 3577688]

Dore-Duffy P, Owen C, Balabanov R, Murphy S, Beaumont T, Rafols JA. Pericyte migration from the vascular wall in response to traumatic brain injury. Microvascular research. 2000; 60:55–69. [PubMed: 10873515]

Drab M, Verkade P, Elger M, Kasper M, Lohn M, Lauterbach B, Menne J, Lindschau C, Mende F, Luft FC, et al. Loss of caveolae, vascular dysfunction, and pulmonary defects in caveolin-1 gene-disrupted mice. Science. 2001; 293:2449–2452. [PubMed: 11498544]

Drew PJ, Shih AY, Driscoll JD, Knutsen PM, Blinder P, Davalos D, Akassoglou K, Tsai PS, Kleinfeld D. Chronic optical access through a polished and reinforced thinned skull. Nat Methods. 2010; 7:981–984. [PubMed: 20966916]

Evans V, Hatzopoulos A, Aird WC, Rayburn HB, Rosenberg RD, Kuivenhoven JA. Targeting the Hprt locus in mice reveals differential regulation of Tie2 gene expression in the endothelium. Physiol Genomics. 2000; 2:67–75. [PubMed: 11015584]

Go AS, Mozaffarian D, Roger VL, Benjamin EJ, Berry JD, Borden WB, Bravata DM, Dai S, Ford ES, Fox CS, et al. Heart disease and stroke statistics--2013 update: a report from the American Heart Association. Circulation. 2013; 127:e6–e245. [PubMed: 23239837]

Gursoy-Ozdemir Y, Yemisci M, Dalkara T. Microvascular protection is essential for successful neuroprotection in stroke. J Neurochem. 2012; 123(Suppl 2):2–11. [PubMed: 23050637]

Itallie CM, Anderson JM. Caveolin binds independently to claudin-2 and occludin. Annals of the New York Academy of Sciences. 2012; 1257:103–107. [PubMed: 22671595]

Ito U, Ohno K, Yamaguchi T, Takei H, Tomita H, Inaba Y. Effect of hypertension on blood-brain barrier. Change after restoration of blood flow in post-ischemic gerbil brains. An electronmicroscopic study. Stroke. 1980; 11:606–611. [PubMed: 7210066]

Jasmin JF, Malhotra S, Singh Dhallu M, Mercier I, Rosenbaum DM, Lisanti MP. Caveolin-1 deficiency increases cerebral ischemic injury. Circ Res. 2007; 100:721–729. [PubMed: 17293479]

Jiao H, Wang Z, Liu Y, Wang P, Xue Y. Specific role of tight junction proteins claudin-5, occludin, and ZO-1 of the blood-brain barrier in a focal cerebral ischemic insult. J Mol Neurosci. 2011; 44:130–139. [PubMed: 21318404]

Krueger M, Hartig W, Reichenbach A, Bechmann I, Michalski D. Blood-brain barrier breakdown after embolic stroke in rats occurs without ultrastructural evidence for disrupting tight junctions. PLoS One. 2013; 8:e56419. [PubMed: 23468865]

Lakhan SE, Kirchgessner A, Tepper D, Leonard A. Matrix metalloproteinases and blood-brain barrier disruption in acute ischemic stroke. Front Neurol. 2013; 4:32. [PubMed: 23565108]

Liu J, Jin X, Liu KJ, Liu W. Matrix metalloproteinase-2-mediated occludin degradation and caveolin-1-mediated claudin-5 redistribution contribute to blood-brain barrier damage in early ischemic stroke stage. J Neurosci. 2012a; 32:3044–3057. [PubMed: 22378877]

Liu S, Agalliu D, Yu C, Fisher M. The role of pericytes in blood-brain barrier function and stroke. Curr Pharm Des. 2012b; 18:3653–3662. [PubMed: 22574979]

Lossinsky AS, Shivers RR. Structural pathways for macromolecular and cellular transport across the blood-brain barrier during inflammatory conditions. Review Histol Histopathol. 2004; 19:535–564.

Luissint AC, Artus C, Glacial F, Ganeshamoorthy K, Couraud PO. Tight junctions at the blood brain barrier: physiological architecture and disease-associated dysregulation. Fluids Barriers CNS. 2012; 9:23. [PubMed: 23140302]

Marchiando AM, Shen L, Graham WV, Weber CR, Schwarz BT, Austin JR 2nd, Raleigh DR, Guan Y, Watson AJ, Montrose MH, Turner JR. Caveolin-1-dependent occludin endocytosis is required for TNF-induced tight junction regulation in vivo. J Cell Biol. 2010; 189:111–126. [PubMed: 20351069]

Morita K, Sasaki H, Furuse M, Tsukita S. Endothelial claudin: claudin-5/TMVCF constitutes tight junction strands in endothelial cells. J Cell Biol. 1999; 147:185–194. [PubMed: 10508865]

Nag S. Morphology and molecular properties of cellular components of normal cerebral vessels. Methods in molecular medicine. 2003; 89:3–36. [PubMed: 12958410]

NIH-PA Author Manuscript NIH-PA Author Manuscript NIH-PA Author Manuscript

Nag S, Venugopalan R, Stewart DJ. Increased caveolin-1 expression precedes decreased expression of occludin and claudin-5 during blood-brain barrier breakdown. Acta Neuropathol. 2007; 114:459–469. [PubMed: 17687559]

Nimmerjahn A. Optical window preparation for two-photon imaging of microglia in mice. Cold Spring Harb Protoc. 2012a; 2012:587–593.

Nimmerjahn A. Surgical implantation of a head plate in mice in preparation for in vivo two-photon imaging of microglia. Cold Spring Harb Protoc. 2012b; 2012

Nimmerjahn A. Two-photon imaging of microglia in the mouse cortex in vivo. Cold Spring Harb Protoc. 2012c; 2012

Nimmerjahn A, Mukamel EA, Schnitzer MJ. Motor behavior activates Bergmann glial networks. Neuron. 2009; 62:400–412. [PubMed: 19447095]

Nitta T, Hata M, Gotoh S, Seo Y, Sasaki H, Hashimoto N, Furuse M, Tsukita S. Size-selective loosening of the blood-brain barrier in claudin-5-deficient mice. J Cell Biol. 2003; 161:653–660. [PubMed: 12743111]

Ohkura Y, Akanuma S, Tachikawa M, Hosoya K. Blood-to-retina transport of biotin via Na+-dependent multivitamin transporter (SMVT) at the inner blood-retinal barrier. Exp Eye Res. 2010; 91:387–392. [PubMed: 20599968]

Piontek J, Winkler L, Wolburg H, Müller SL, Zuleger N, Piehl C, Wiesner B, Krause G, Blasig IE. Formation of tight junction: determinants of homophilic interaction between classic claudins. FASEB J. 2008; 22:146–158. [PubMed: 17761522]

Razani B, Engelman JA, Wang XB, Schubert W, Zhang XL, Marks CB, Macaluso F, Russell RG, Li M, Pestell RG, et al. Caveolin-1 null mice are viable but show evidence of hyperproliferative and vascular abnormalities. J Biol Chem. 2001; 276:38121–38138. [PubMed: 11457855]

Rosenberg GA, Yang Y. Vasogenic edema due to tight junction disruption by matrix metalloproteinases in cerebral ischemia. Neurosurgical focus. 2007; 22:E4. [PubMed: 17613235]

Sandoval KE, Witt KA. Blood-brain barrier tight junction permeability and ischemic stroke. Neurobiol Dis. 2008; 32:200–219. [PubMed: 18790057]

Schaffer CB, Friedman B, Nishimura N, Schroeder LF, Tsai PS, Ebner FF, Lyden PD, Kleinfeld D. Two-photon imaging of cortical surface microvessels reveals a robust redistribution in blood flow after vascular occlusion. PLoS Biol. 2006; 4:e22. [PubMed: 16379497]

Schubert W, Frank PG, Razani B, Park DS, Chow CW, Lisanti MP. Caveolae-deficient endothelial cells show defects in the uptake and transport of albumin in vivo. J Biol Chem. 2001; 276:48619–48622. [PubMed: 11689550]

Schubert W, Frank PG, Woodman SE, Hyogo H, Cohen DE, Chow CW, Lisanti MP. Microvascular hyperpermeability in caveolin-1 (−/−) knock-out mice. Treatment with a specific nitric-oxide synthase inhibitor, L-NAME, restores normal microvascular permeability in Cav-1 null mice. J Biol Chem. 2002; 277:40091–40098. [PubMed: 12167625]

Shen L, Weber CR, Turner JR. The tight junction protein complex undergoes rapid and continuous molecular remodeling at steady state. J Cell Biol. 2008; 181:683–695. [PubMed: 18474622]

Simionescu M, Popov D, Sima A. Endothelial transcytosis in health and disease. Cell and tissue research. 2009; 335:27–40. [PubMed: 18836747]

Stamatovic SM, Keep RF, Wang MM, Jankovic I, Andjelkovic AV. Caveolae-mediated internalization of occludin and claudin-5 during CCL2-induced tight junction remodeling in brain endothelial cells. J Biol Chem. 2009; 284:19053–19066. [PubMed: 19423710]

Tiruppathi C, Naqvi T, Wu Y, Vogel SM, Minshall RD, Malik AB. Albumin mediates the transcytosis of myeloperoxidase by means of caveolae in endothelial cells. Proc Natl Acad Sci USA. 2004; 101:7699–7704. [PubMed: 15136724]

Umeda K, Ikenouchi J, Katahira-Tayama S, Furuse K, Sasaki H, Nakayama M, Matsui T, Tsukita S, Furuse M, Tsukita S. ZO-1 and ZO-2 independently determine where claudins are polymerized in tight-junction strand formation. Cell. 2006; 126:741–754. [PubMed: 16923393]

Zlokovic BV. The blood-brain barrier in health and chronic neurodegenerative disorders. Neuron. 2008; 57:178–201. [PubMed: 18215617]

NIH-PA Author Manuscript

NIH-PA Author Manuscript

NIH-PA Author Manuscript

Highlights

- Transgenic *eGFP-Claudin5* mice enable continual time-lapse imaging of BBB TJs.
- TJ structural abnormalities are present at late but not early phases after stroke.
- EC endocytosis and transcytosis are both increased at early phases post-stroke.
- Stroke impairs progressively the transcellular then paracellular endothelial barrier.

NIH-PA Author Manuscript

NIH-PA Author Manuscript

NIH-PA Author Manuscript

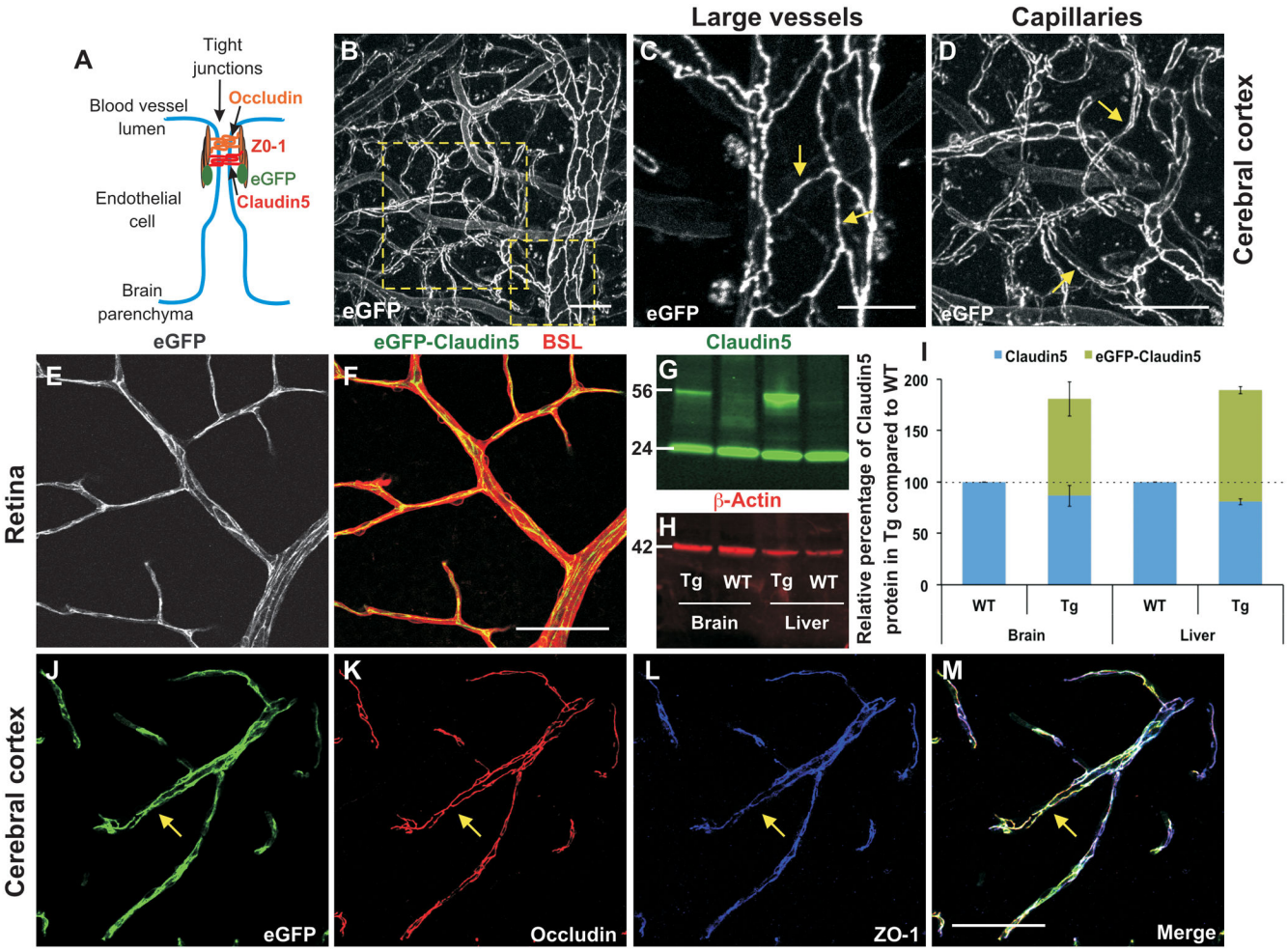

Figure 1. Genetic labeling of endothelial tight junctions with eGFP

(A) Diagram of eGFP-Claudin5 fusion protein localization within endothelial cells (ECs) in transgenic mice. (B–D) Maximum intensity projection images showing 120 μm thick cortical volumes recorded with two-photon microscopy in an anesthetized *Tg eGFP-Claudin5* transgenic mouse. eGFP labels TJs between ECs in venules (B, small yellow rectangle; C, yellow arrows) and capillaries (B, large yellow rectangle; D; yellow arrows). (E, F) Visualization of TJs in retinal blood vessels with eGFP. *Griffonia* (*Bandeiraea*) *simplicifolia* Lectin I (BSL) labels blood vessels (F). (G, H) Western blots with brain and liver lysates from *Tg eGFP-Claudin5* and wild-type mice for Claudin5 (G) and β-actin (H; 42 kDa). The eGFP-Claudin5 fusion is approximately 56 kDa and wild-type Claudin5 is 24 kDa. (I) Quantitation of relative amounts of Claudin5 protein in transgenic and wild-type mice. Levels of Claudin5 protein in wild-type mice were used as a standard (100 percent, dotted line, blue bars). Levels of Claudin5 protein in transgenic mice are presented as a percentage of protein levels in wild-type mice, each being normalized to its respective β-actin control. Transgenic animals have almost twice the amount of Claudin5 protein, from both the endogenous locus (blue bars) and the transgene (green bars). (J–M) The fusion protein is localized to TJs in brain ECs, together with Occludin and ZO-1. See Figure S1 for expression of the fusion protein in other organs. Scale bars = 50 μm.

NIH-PA Author Manuscript

NIH-PA Author Manuscript

NIH-PA Author Manuscript

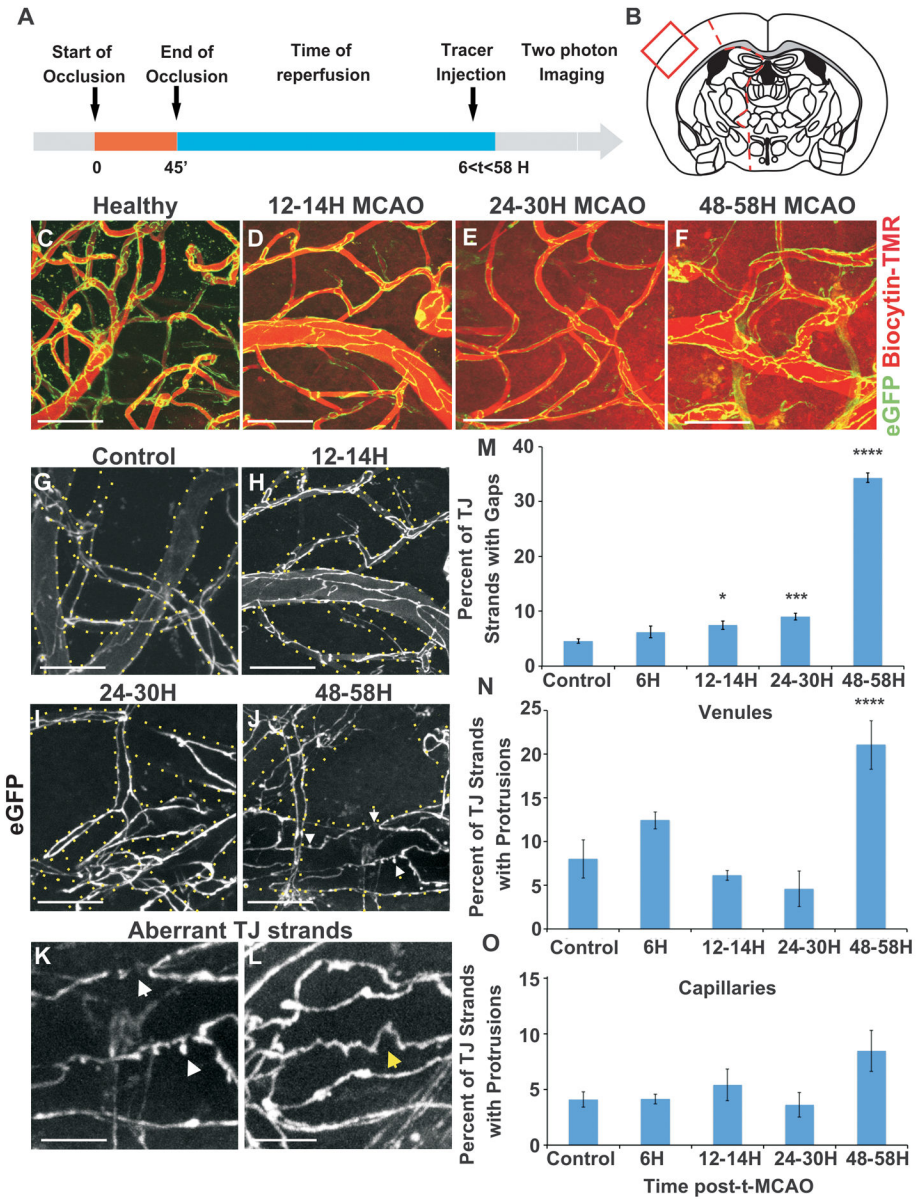

Figure 2. Integrity of cortical blood vessel TJs is impaired at late but not early time points following stroke in live *Tg eGFP-Claudin5* mice

(A, B) Diagram of the experimental procedure and cortical region where *in vivo* two-photon imaging was performed in *Tg eGFP-Claudin5* mice. (C–F) Maximum intensity projections of 120 μm thick cortical volumes from healthy mouse brain (C) and 12–14 h (D), 24–30 h (E) and 48–58 h (F) after t-MCAO obtained with two-photon imaging through a cranial window. The imaging areas were located within the stroke core region (D–F). eGFP labels TJs. Biocytin-TMR tracer leakage from blood vessels into the CNS parenchyma was visualized 30 min after tail vein injection in E, F (red background). (G–L) Maximum intensity projections of 120 μm thick cortical volumes showing TJs in venules and capillaries of healthy control (G) and diseased mice 12–14 h (H), 24–30 h (I), and 48–58 h (J–L) following t-MCAO. Notice the presence of gaps (J, K; white arrows), protrusions (J,

NIH-PA Author Manuscript

NIH-PA Author Manuscript

NIH-PA Author Manuscript

K; arrowheads) and aberrant zigzag TJ morphology (L, yellow arrow) at 48–58 h. Yellow dots indicate blood vessel boundaries outlined by the presence of the tracer (data not shown for simplicity). (M–O) Bar graphs showing the percent of TJ strands with gaps (M) and protrusions in venules (N) and capillaries (O) during stroke progression. The fraction of TJ strands with gaps or protrusions in venules, but not capillaries, is significantly different 48–58 h post-t-MCAO compared to the control. Data were collected from 2–8 independent fields of view (377 μm × 377 μm) that contained between 61–183 TJ strands in either venules or capillaries from the imaging area (n = 3–5 transgenic animals per time point). Data are represented as mean ± s.e.m, * $p<0.05$; *** $p<0.001$, ****$p<0.0001$, mixed effect ANOVA. See Figure S2 for a quantitative comparison of biocytin-TMR and IgG leakage during stroke progression in wild-type vs. *Tg eGFP-Claudin5* mice and Movies S1–S2. Scale bar = 50 μm (C–J), 25 μm (K, L).

NIH-PA Author Manuscript

NIH-PA Author Manuscript

NIH-PA Author Manuscript

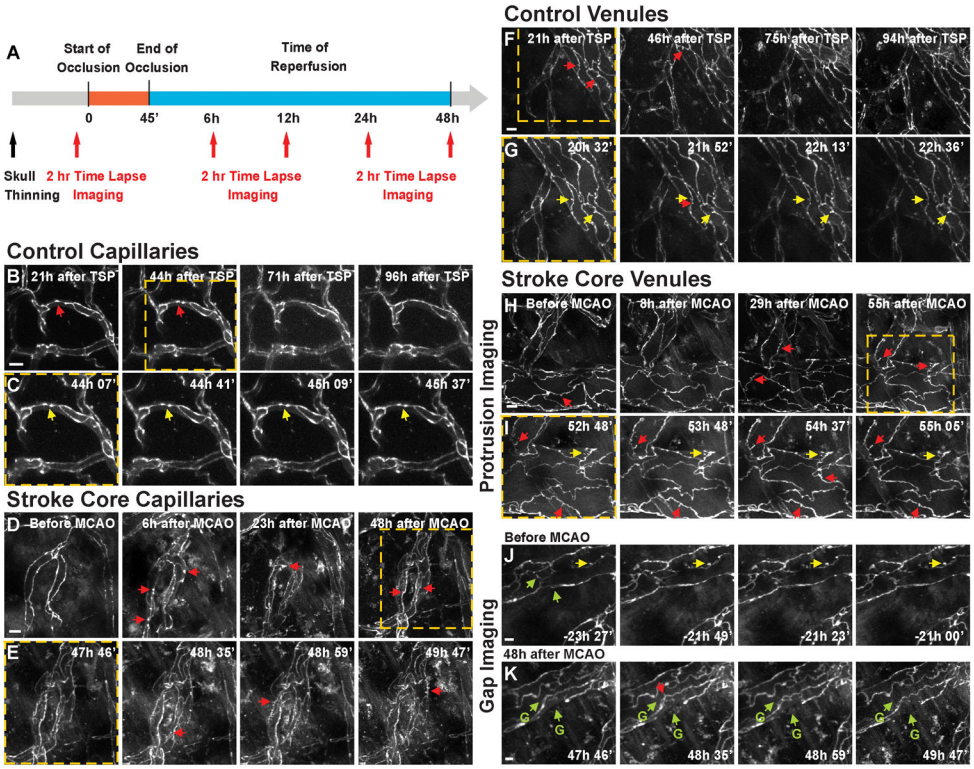

Figure 3. Continual two-photon time-lapse imaging of cortical endothelial TJs in healthy and diseased *Tg eGFP-Claudin5* mice reveals that protrusions but not gaps are highly dynamic 48–58 h post t-MCAO

(A) Diagram of the experimental procedure for transcranial two-photon time-lapse imaging of *Tg eGFP-Claudin5* mice. Four imaging sessions were conducted in both control and stroke animals. Each session lasted ~2 h and involved repeated optical recordings (every 15–25 min) from distinct cortical volumes. Stroke animals were imaged once before and three times after t-MCAO (~6 h or 12 h, then ~24 h and 48 h). Controls were imaged at corresponding time points. Imaging began ~24 h after thinned skull preparation (TSP). (B–E) Sample time-lapse images of eGFP$^+$ TJs in cortical capillaries from control (B, C) or stroke animals (D, E). Images in B and D are from different days/imaging sessions, images in C and E from a selected day/imaging session (yellow boxed region in B and D). Stroke images (D, E) are from the stroke core region, verified *post hoc* 48–60 h post t-MCAO by tracer leakage into the parenchyma (data not shown). Cortical capillaries show very few protrusions in both healthy and stroke core tissue. Protrusions are particularly dynamic during the 47–50 h period after t-MCAO. (F–I) Time-lapse imaging example of eGFP$^+$ TJs in cortical venules from control (F, G) or stroke animals (H, I; stroke core region). Venule protrusions are highly dynamic at several time points after t-MCAO and within the highlighted two-hour time-lapse period. Venules also have more protrusions than capillaries. Static protrusions present in all images are labeled in yellow, dynamic protrusions are labeled in red. (J, K) Time-lapse images of a venule before (J) and after (K) stroke illustrating gap formation (green arrows with letter G). See also Movies S3–S8 and Figure S3 for time-lapse images from the penumbra region. Scale bars = 10 μm (B–K).

NIH-PA Author Manuscript

NIH-PA Author Manuscript

NIH-PA Author Manuscript

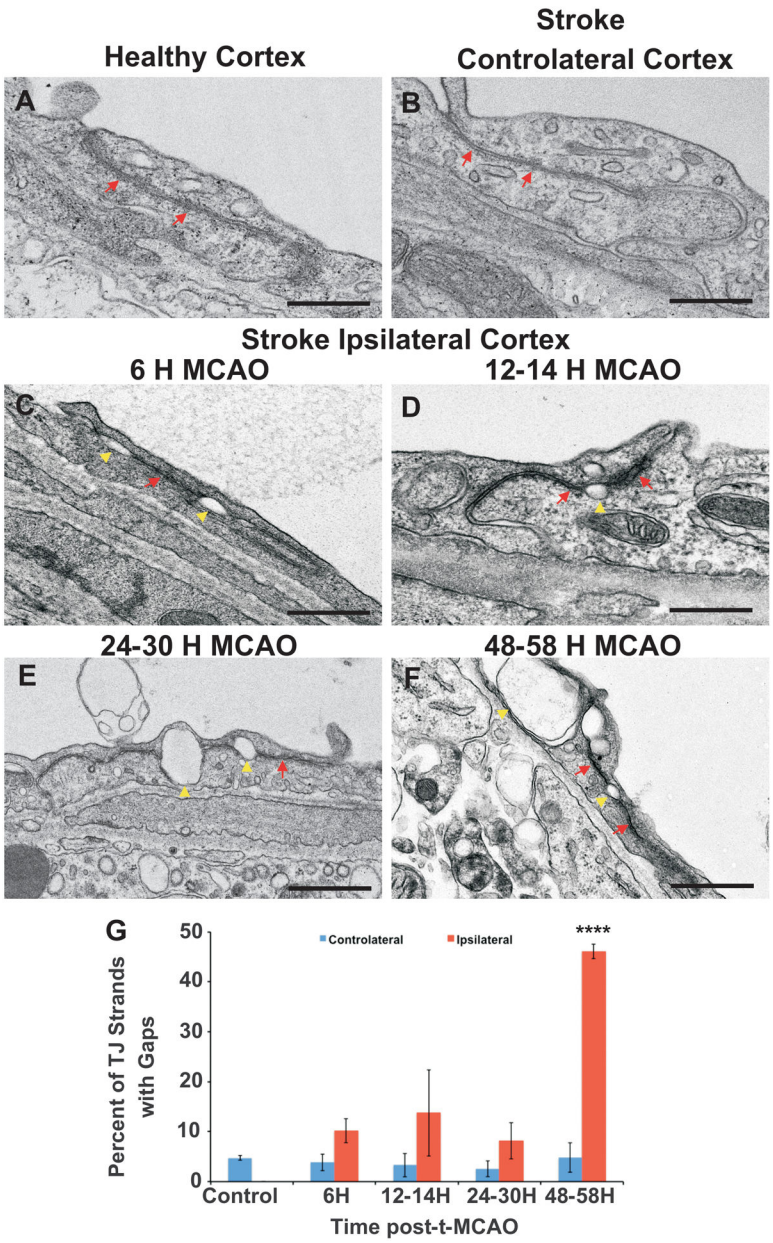

Figure 4. Ultrastructural changes in endothelial TJs appear at late but not early time points following t-MCAO in *Tg eGFP-Claudin5* mice

(A–F) Transmission electron microscopy (TEM) of TJs in ECs from healthy (A), contralateral (24 h post-t-MCAO; B) and ipsilateral stroke cortex at 6 h (C), 12–14 h (D), 24–30 h (E) and 48–58 h (F) post-t-MCAO. Note structurally abnormal TJs that contain large gaps (yellow arrows) within normal regions (red arrows) in particular 24–30 h and 48–58 h post-t-MCAO. (G) Bar graphs showing the fraction of TJ strands with gaps during stroke progression after t-MCAO from TEM analysis. The proportion of TJ strands with gaps is significantly different 48–58 h post-t-MCAO as compared to other groups. Data were collected from 65–70 independent fields of view (2.6 μm × 1.7 μm) that contained between 1–3 TJ strands in either venules or capillaries (n = 2–5 transgenic animals per time

point). Data are represented as mean ± s.e.m, ****p<0.0001, one-way ANOVA. Scale bars = 400 nm. See Figure S4 for analysis of TJ and basement membrane protein expression during stroke in *Tg eGFP-Claudin5* mice.

NIH-PA Author Manuscript
NIH-PA Author Manuscript
NIH-PA Author Manuscript

NIH-PA Author Manuscript

NIH-PA Author Manuscript

NIH-PA Author Manuscript

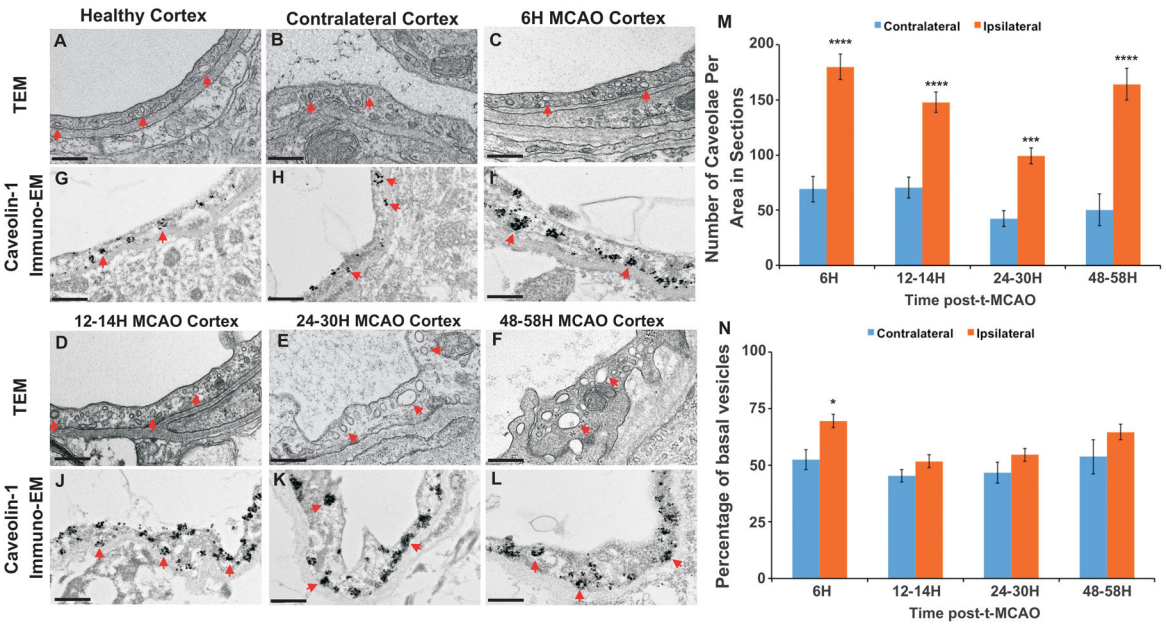

Figure 5. Early increase in endothelial caveolae within the cortical stroke region from *Tg eGFP-Claudin5* mice following t-MCAO

(A–F) TEM of cortical ECs in healthy (A), contralateral (24 h post-t-MCAO; B) and ipsilateral stroke cortex at 6 h (C), 12–14 h (D), 24–30 h (E) and 48–58 h (F) post-t-MCAO. The vesicle number in ECs (red arrows) is increased as early as 6 h post-t-MCAO and remains above the control baseline up to 58 h post-t-MCAO. (G–L) Immuno-EM for Caveolin-1 in healthy (G), contralateral (H) and ipsilateral stroke cortex 6 h (I), 12–14 h (J), 24–30 h (K) and 48–58 h (L) post t-MCAO. The number of Cav-1^{+} vesicles (red arrows) is significantly increased in the stroke cortex at all time points. (M) Bar graph of the number of Cav1^{+} caveolae per area from immuno-EM images during stroke progression. The number of caveolae in each section is significantly higher in the ipsilateral (stroke; orange bars) versus contralateral (blue bars) cortex. (N) Bar graph of the basal distribution of Cav1^{+} caveolae in endothelial cells within the imaged area during stroke progression. Caveolae are found more frequently at the basal side of the endothelium in the ipsilateral (orange bars) versus contralateral (blue bars) cortex. Data were accumulated from 20–95 independent fields of view (2.6 μm × 1.7 μm) that contained between 1–4 ECs from venules or capillaries either within the cortical stroke core or contralateral region (n = 2–5 transgenic animals per time point). Data are represented as mean ± s.e.m, *$p < 0.05$, ***$p < 0.001$, ****$p < 0.0001$, one-way ANOVA. Scale bars = 400 nm.

NIH-PA Author Manuscript

NIH-PA Author Manuscript

NIH-PA Author Manuscript

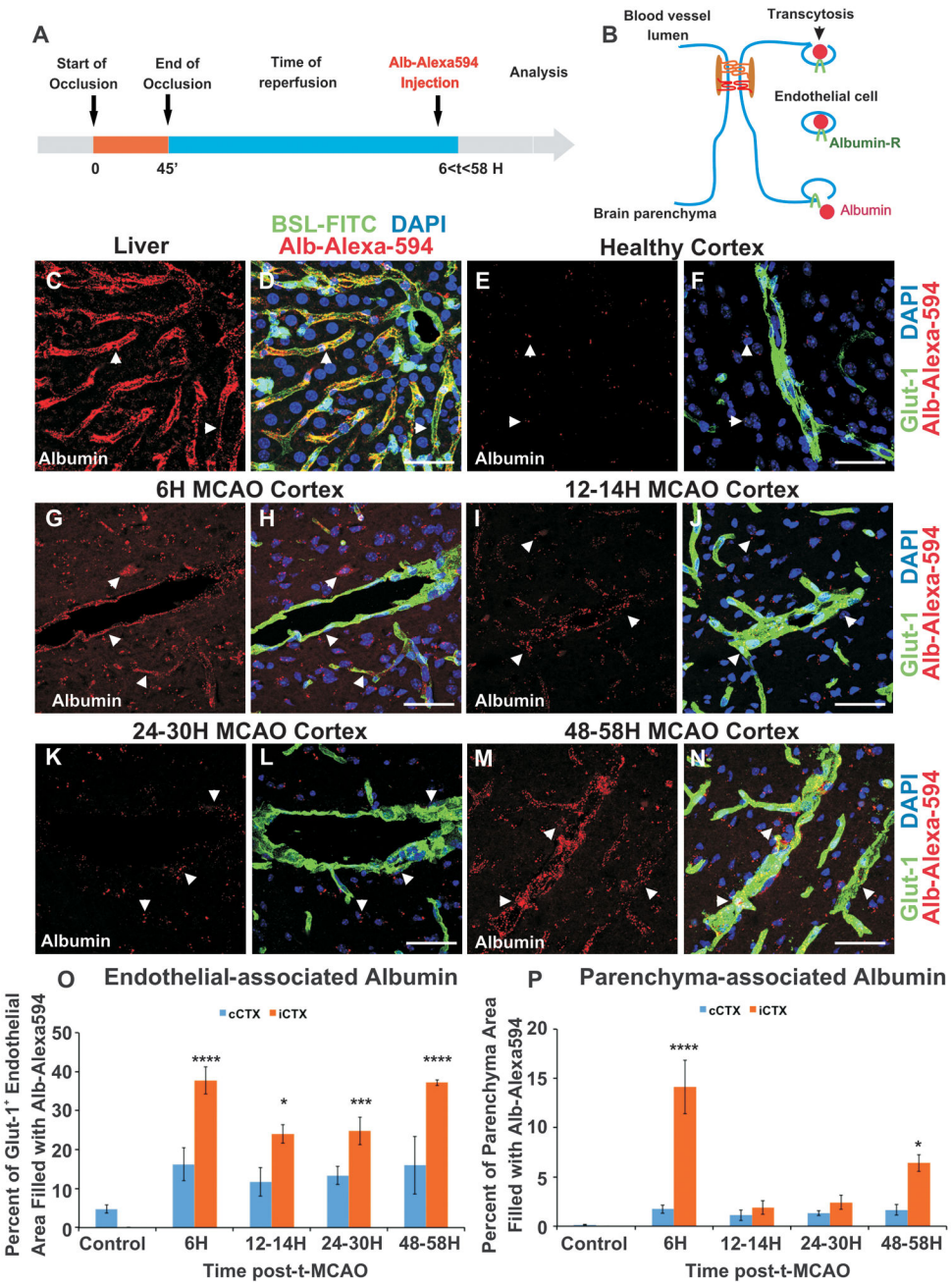

Figure 6. Increased endocytosis and transcytosis rates in brain endothelium occur as early as 6 h post-t-MCAO

(A, B) Diagrams of the experimental procedure (A) and labeling of caveolae and other transcytosis vesicles with albumin-Alexa594 (alb-Alexa594; B). (C–N) Uptake of alb-Alexa594 in liver (C, D), healthy cortex (E, F) and ipsilateral stroke cortex from 6–48 h post-t-MCAO (G–N). Note the increase in alb-Alexa594 uptake within CNS endothelium labeled with Glut-1 as early as 6 h post-t-MCAO. Liver ECs are marked with BSL (green; D) and brain ECs with Glut-1 (F, H, J, L, N) in merged panels. Note the increase in alb-Alexa594 uptake within CNS endothelium as early as 6 h post-t-MCAO. (O–P) Bar graphs

NIH-PA Author Manuscript

NIH-PA Author Manuscript

NIH-PA Author Manuscript

showing the percentage of Glut-1^{+} endothelial (O) or brain parenchyma (P) area filled with alb-Alexa594 in ipsilateral (orange) and contralateral (blue) cortex. The fraction of endothelial- and parenchyma-filled area with alb-Alexa594 is significantly higher at 6 h and 48 hours post-t-MCAO compared to healthy cortex. Data were collected from 4–9 independent fields of view that contained cortical venules or capillaries (n = 3–5 animals per time point). Data are represented as mean ± s.e.m, *$p<0.05$; ****$p<0.0001$, mixed effect ANOVA. Scale bars = 50 μm. See Figure S5 for analysis of percent of BSL^{+} endothelial or parenchyma area filled with alb-Alexa594 in ipsilateral and contralateral cortex.

NIH-PA Author Manuscript

NIH-PA Author Manuscript

NIH-PA Author Manuscript

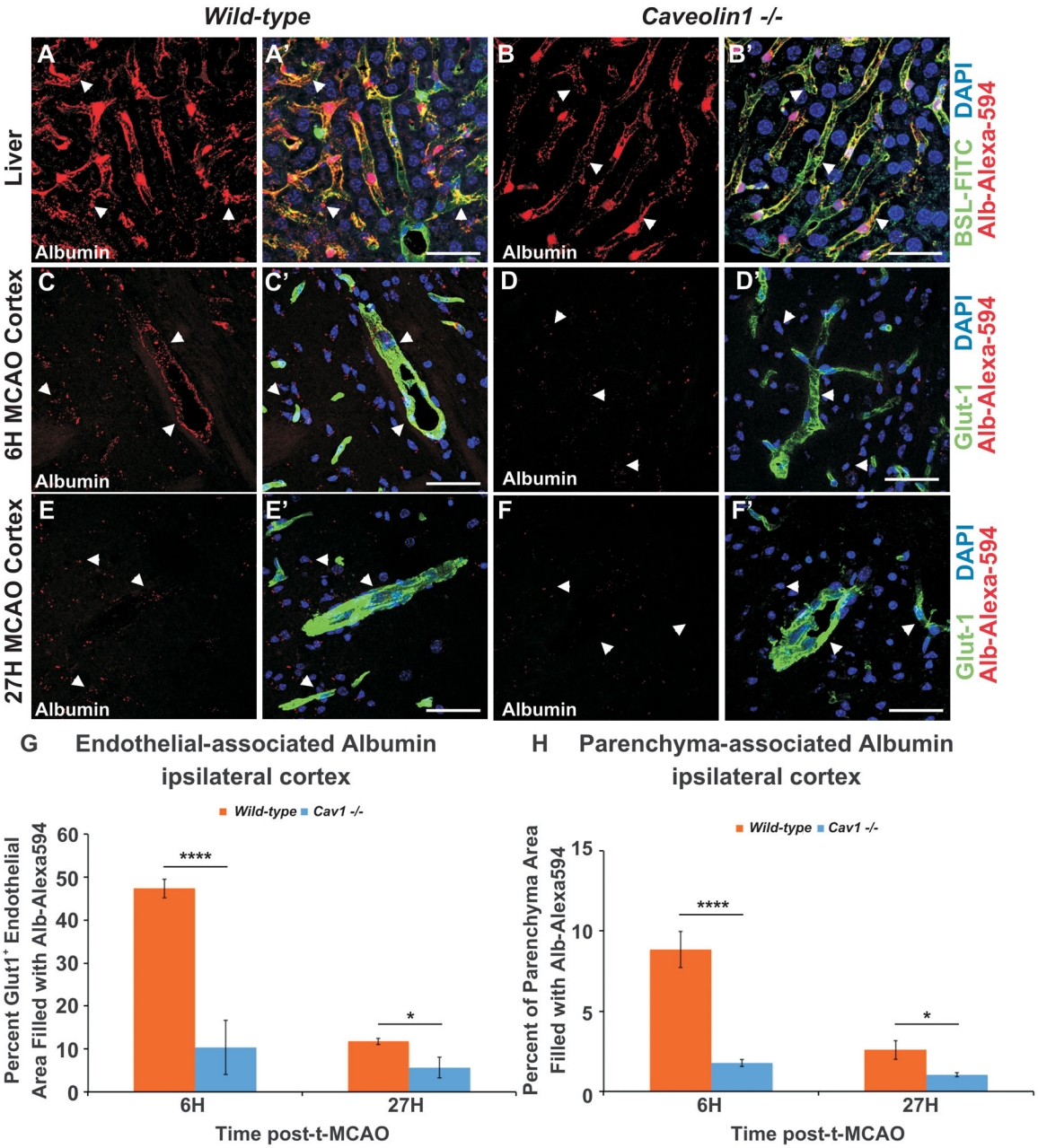

Figure 7. Reduced endothelial endocytosis and transcytosis in Caveolin1-deficient mice in response to stroke

(A–F′) Uptake of alb-Alexa594 in liver (A–B′) and ipsilateral stroke cortex (C–F′) 6 h and 27 h post-t-MCAO in wild-type or *Cav1*$^{-/-}$ mice. Note the decrease in alb-Alexa594 uptake by ECs in liver or ipsilateral cortex for mutant versus wild-type mice. Liver ECs are labeled with BSL-FITC (green; A–B′) and brain ECs with Glut1 (green; C–F′) in merged panels. (G–H) Bar graphs showing the fraction of Glut1^{+} endothelial (G) or parenchymal (H) area filled with alb-Alexa594 in the ipsilateral cortex of wild-type (orange) or *Cav1*$^{-/-}$ mice (blue), 6 h and 27 h post t-MCAO. The percentage of endothelial and parenchymal area filled with alb-Alexa594 is significantly reduced 6 h and 27 hours post-t-MCAO in Cav-1$^{-/-}$

NIH-PA Author Manuscript

NIH-PA Author Manuscript

NIH-PA Author Manuscript

mice compared to controls. Data were collected from 4–9 independent fields of view that contain cortical venules or capillaries from wild-type (n = 3) or *Cav1*$^{-/-}$ (n = 3) mice per time point. Data are represented as mean ± s.e.m, *p<0.05; ****p<0.0001, paired t-test. Scale bars = 50 μm (A–F′). See Figure S6 for quantitative analysis of the fraction of BSL^{+} endothelial or parenchymal area filled with alb-Alexa594 in the ipsilateral cortex from wild-type or *Cav1*$^{-/-}$ mice, 6 h and 27 h post t-MCAO, and characterization of Alb^{+} Cav1^{-} vesicles in primary brain endothelial cells.

NIH-PA Author Manuscript

NIH-PA Author Manuscript

NIH-PA Author Manuscript

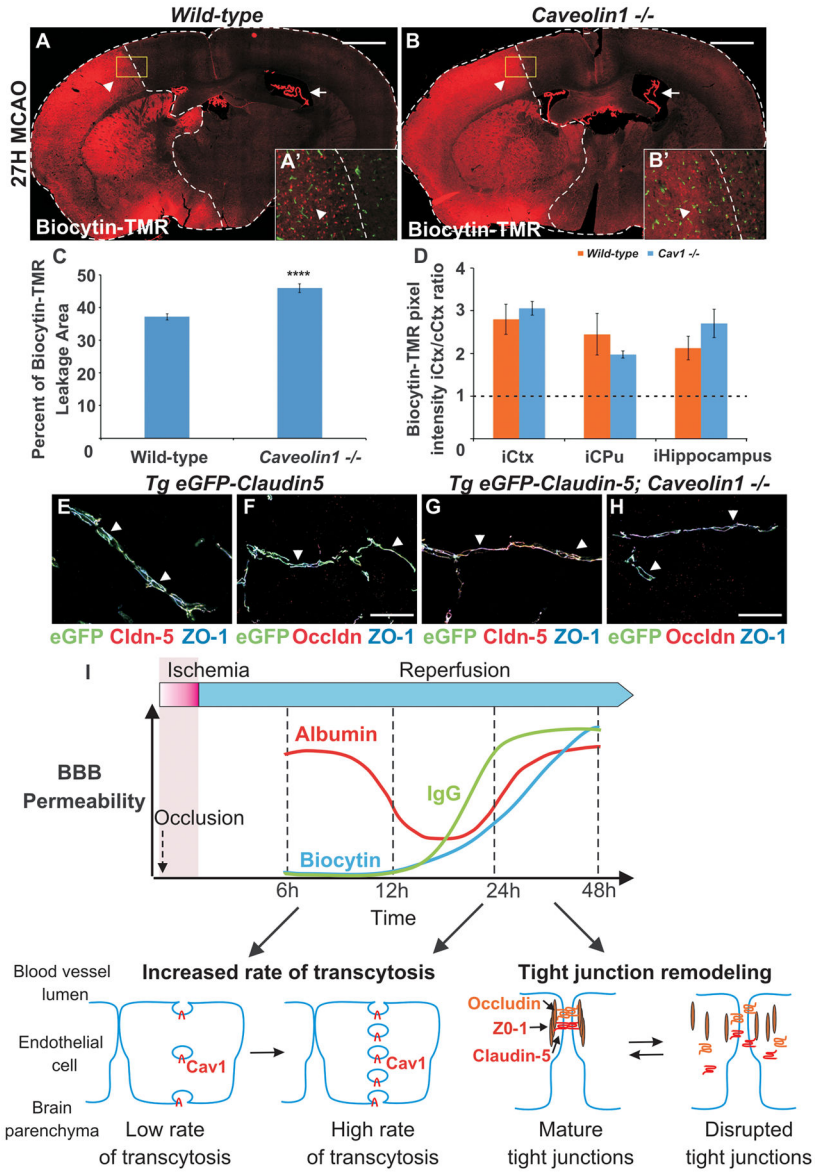

Figure 8. Cav1-deficient mice exhibit an increase in paracellular endothelial permeability similar to wild-type mice following t-MCAO

(A –B) Brain sections from wild-type (A) or *Cav1*$^{-/-}$ (B) mice showing Biocytin-TMR leakage 27 h post-t-MCAO. The area of biocytin-TMR leakage and the outline of the brain section are marked with dashed white lines. Note the extensive leakage of tracer into the cortex and putamen. The choroid plexus (A, B; arrows) is intensely labeled due to lack of the barrier. (A′, B′) Higher magnification images for the yellow squares shown in (A, B). (C) Bar graph showing the fraction of biocytin-TMR leakage area in wild-type or *Cav1*$^{-/-}$ mice. The increased fraction of biocytin-TMR areas in mutant mice is due to tracer in the thalamus. (D) Bar graphs of the biocytin-TMR average pixel intensity ratio between ipsilateral and contralateral areas for cortex, putamen and hippocampus in wild-type (orange bars) or *Cav1*$^{-/-}$ mice (blue bars). There is no significant difference in biocytin-TMR leakage intensity for matched anatomical regions. Data are represented as mean ± s.e.m,

NIH-PA Author Manuscript

NIH-PA Author Manuscript

NIH-PA Author Manuscript

****p<0.0001, paired t-test. (E–H) Expression of eGFP-Claudin5, Claudin5, Occludin and ZO-1 in *Tg eGFP-Claudin5* (E, F) and *Tg eGFP-Claudin5 Cav1*$^{-/-}$ mice (G, H). TJ proteins are correctly localized in CNS ECs of both strains. (I) Schematic representation of increases in biocytin-TMR (blue), IgG (green) and alb-Alexa594 (red) over time following t-MCAO. There is a non-linear, gradual increase in biocytin-TMR and IgG permeability during stroke progression that becomes significant 24–48 h after t-MCAO, and correlates with the abundance of structural defects in TJs (i.e. junction remodeling). In contrast, alb-Alexa594 uptake increases as early as 6 h post-t-MCAO, suggesting that endocytosis and transcytosis are increased in early phases of ischemic stroke. Upregulation of both Cav1-dependent and -independent endothelial transcytosis, followed by TJ disassembly, contribute to enhanced BBB permeability after t-MCAO. Scale bars = 400 μm (A, B) and 50 μm (E–H). See Figure S7 for analysis of IgG leakage after stroke, the morphology of TJs with TEM and TJ protein levels in wild-type versus *Cav1*$^{-/-}$ brains.